ACS APPLIED MATERIALS & INTERFACES

www.acsami.org

Research Article

# Performance of Quaternized Polybenzimidazole-Cross-Linked Poly(vinylbenzyl chloride) Membranes in HT-PEMFCs

Funda Arslan,* Khajidkhand Chuluunbandi, Anna T.S. Freiberg, Attila Kormanyos, Ferit Sit, Serhiy Cherevko, Jochen Kerres, Simon Thiele, and Thomas Böhm*

Cite This: *ACS Appl. Mater. Interfaces* 2021, 13, 56584–56596

Read Online

ACCESS | Metrics & More | Article Recommendations | Supporting Information

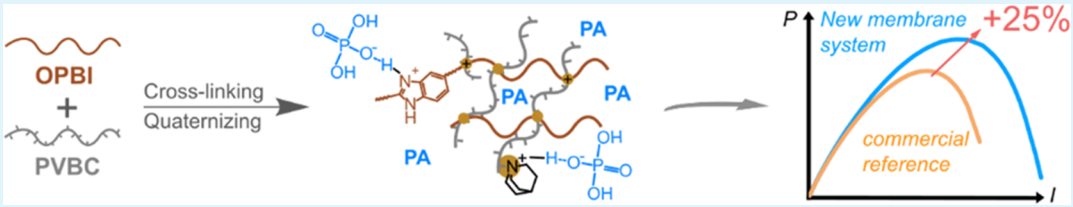


**ABSTRACT:** High-temperature proton-exchange membrane fuel cells (HT-PEMFCs) are mostly based on acid-doped membranes composed of polybenzimidazole (PBI). A severe drawback of acid-doped membranes is the deterioration of mechanical properties upon increasing acid-doping levels. Cross-linking of different polymers is a way to mitigate stability issues. In this study, a new ion-pair-coordinated membrane (IPM) system with quaternary ammonium groups for the application in HT-PEMFCs is introduced. PBI cross-linked with poly(vinylbenzyl chloride) and quaternized with three amines (DABCO, quinuclidine, and quinuclidinol) are manufactured and compared to the state-of-the-art commercial Dapazol PBI membrane *ex situ* as well as by evaluating their HT-PEMFC performance. The IPMs show reduced swelling and better mechanical properties upon doping, which enables a reduction in membrane thickness while maintaining a comparably low gas crossover and mechanical stability. The HT-PEMFC based on the best-performing IPM reaches up to 530 mW $cm^{-2}$ at 180 °C under $H_2$/air conditions at ambient pressure, while Dapazol is limited to less than 430 mW $cm^{-2}$ at equal parameters. This new IPM system requires less acid doping than conventional PBI membranes while outperforming conventional PBI membranes, which renders these new membranes promising candidates for application in HT-PEMFCs.

**KEYWORDS:** *Proton-exchange membrane, phosphoric acid, ion pair, high-temperature proton-exchange membrane fuel cell, quaternary ammonium groups, hydrogen gas crossover*



## 1. INTRODUCTION

Fuel cells (FCs) are promising energy conversion devices, gaining more importance with the world's increasing energy demand and the need to reduce $CO_2$ emission. Among different types of FCs, proton-exchange membrane FCs (PEMFCs) are the most promising and best developed due to their applicability in different areas such as the automotive application and in the energy storage sector.[1,2] PEMFCs can be divided into low-temperature (LT) PEMFCs (below 100 °C) and high-temperature (HT) PEMFCs (above 100 °C).[1] HT-PEMFCs offer various advantages over LT-PEMFCs, such as faster reaction kinetics and improved tolerance to carbon monoxide (CO).[1,3−5] Above 100 °C, no liquid water management is required when operating at ambient pressure, and the higher temperature simplifies the cooling system by the larger difference between FC and ambient temperature.[6]

Membranes used in LT-PEMFC application are mainly based on perfluorosulfonic acid polymers such as Nafion. Their proton conductivity depends on humidification, and therefore, these types of proton-exchange membranes (PEMs) lose ionic conductivity above 100 °C.[7] In this regard, basic polymers doped with nonvolatile inorganic acids have proven themselves as efficient HT-PEMs.[1] Polybenzimidazole (PBI) is currently the polymer of choice for HT-PEMFCs when doped with phosphoric acid (PA, $H_3PO_4$).[8] Among different types of PBIs, the most investigated as HT-PEM is poly[2,2′-(*m*-phenylene)-5,5′-(bibenzimidazole)] (*m*-PBI) (see Figure S1), which is also commercially available in different forms such as coatings or fibers.[1,9] PBI shows excellent thermal and chemical stability, with a glass transition temperature above 400 °C.[6,10] Two basic N-sites per repeating unit can interact with PA molecules. Additionally, free PA molecules will enter the PBI polymer matrix and generate the main proton conductive network. The proton conduction in PBI/PA systems depends on the

Received: September 6, 2021
Accepted: October 29, 2021
Published: November 16, 2021

protonation equilibrium of the acid by building a network of $N-H^+\cdots H_2PO_4^-$, $H_3PO_4\cdots H_2PO_4^-$, and/or $N-H^+\cdots H-OH$, which enables proton hopping.[11−13,48]

Since PA is responsible for proton conductivity in HT-PEMs, the acid-doping level (ADL), which is defined as the number of PA molecules per repeating unit of the basic polymer, is a crucial parameter for HT-PEMFC performance.[12] While higher ADLs increase proton conductivity, they also deteriorate the mechanical strength of the membrane.[4−6,12] Alternatively, an acid uptake (AU) instead of the ADL is provided, which corresponds to the weight gain due to PA uptake relative to the dry weight of the membrane.[14] The AU is the preferred measure of the acid content for cross-linked HT-PEMs. This type of composite membrane includes not only a basic polymer such as PBI but also an additional polymer that is covalently or ionically cross-linked with the basic polymer. Cross-linked membranes aim at maintaining mechanical stability upon acid doping, enhancing chemical stability and degradation resistance, and lowering the acid loss of PEMs at high PA-doping levels.[11,15−20]

Ionic cross-links are formed by mixing a basic PBI-type polymer with acidic polymers (*e.g.*, sulfonated polysulfones).[11,21] Covalent cross-linking can be achieved by using, for example, low-molecular compounds such as divinyl sulfone,[22] bisphenol A-diepoxide,[23] terephthaldehyde,[24] or dichloromethyl phosphinic acid.[21,25] Also, macromolecular cross-linkers are well-established in the literature, such as halomethylated polymers,[26] chloromethylated PSU,[27] bromomethylated polyetherketone,[28] or poly(vinylbenzyl chloride) (PVBC).[21,29]

Recently, PEMs containing quaternary ammonium (QA) functional groups are gaining significant attention for the application in HT-PEMFCs.[1] When doped with PA for use as an HT-PEM, these membrane systems are called ion-pair-coordinated membranes (IPMs). The QA moieties can form strong interactions with biphosphate anions.[11] These additional interactions can prevent PA leaching since the QA$\cdots H_2PO_4^-$ interaction is 8 times stronger than the acid−base interaction between benzimidazole and PA.[15,30] In 2011, Ma et al. evaluated poly(arylene ether ketone) with pendant QA groups and doped with PA as HT-PEMs. Their results showed that QA groups show a better PA-doping ability than the imidazole groups in PBI while maintaining thermal and mechanical stability.[31] In 2014, Cho et al. cross-linked *m*-PBI with methylated PBI-OO bearing two QA groups. A stronger PA absorption for these membranes could be observed.[32] Furthermore, Lee et al. presented in 2016 a QA-biphosphate ion-pair-coordinated polyphenylene membrane that yielded a peak power density of 800 mW $cm^{-2}$ at 180 °C during $H_2/O_2$ operation.[33] Using the same membrane material, Atanasov et al. recently optimized the catalyst layer of an HT-PEMFC using a phosphonated ionomeric binder, yielding peak power densities between 309 and 923 mW $cm^{-2}$ at 120−240 °C under $H_2$/air conditions. At 160 °C and at a current density of approximately 1600 mA $cm^{-2}$, a peak power density of 540 mW $cm^{-2}$ was achieved.[34] Hu et al. investigated PBIs with macromolecular hyperbranched cross-linkers and QA as HT-PEMs.[15] They cross-linked bromomethylated poly(p-xylene) with poly(4,4′-diphenylether-5,5′-bibenzimidazole) (OPBI) and used trimethylamine as a quaternizing agent. Their results showed that the basic QA moieties helped to dissociate PA, establishing acid−base pairs, which enhanced proton conductivity and acid retention. They reported a peak power density of 260 mW $cm^{-2}$ at 160 °C during $H_2$/air operation.

A potentially good amine for the application in IPMs is 1,4-diazabicyclo(2.2.2)octane (DABCO) (see Figure 1), which is, for example, known for its use in the research field of anion-exchange membranes.[35,36] In this work, its performance as a quaternizing agent for OPBI-*c*-PVBC cross-linked membrane systems for the application in HT-PEMFCs was investigated. Furthermore, the amines 1-azabicyclo(2.2.2)octan-3-ol (quinuclidinol) and 1-azabicyclo(2.2.2)octane (quinuclidine) (see Figure 1) were chosen as structural relatives to DABCO. The main difference between these three amines is the number of amine moieties (see Figure 1). The main difference between quinuclidine and quinuclidinol is the −OH group present in the latter, which may contribute to the hydrogen-bonding network between PA and its anions, leading to stronger interactions and less PA leaching.

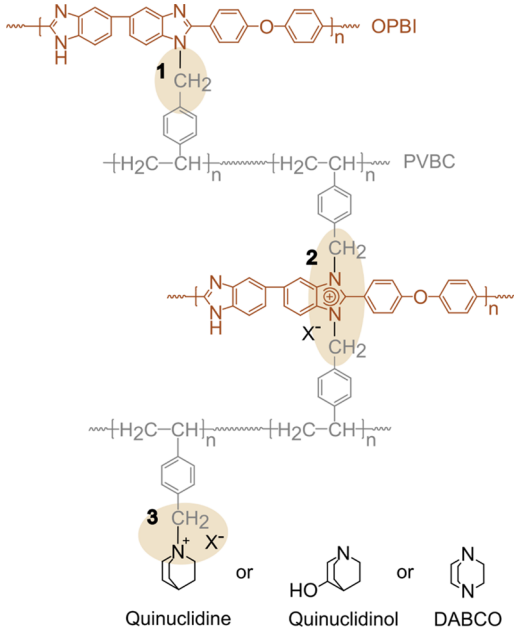


**Figure 1.** Chemical structures of the three amines (quinuclidine, quinuclidinol, and DABCO) and the polymer blend membrane OPBI-*c*-PVBC (exemplary for quinuclidine). Cross-linking points are highlighted and numbered (1: covalent cross-linking, 2: imidazolium cation ($Im^+$), and 3: QA). $X^-$ represents the counter anion, for example, $Cl^-$, $OH^-$, and $H_2PO_4^-$.

In this work, we study the effect of these three amines on cross-linked membranes comprising OPBI and PVBC in three different ratios. The prepared membranes were evaluated *ex situ* as well as within an HT-PEMFC. As a reference system, the commercial HT membrane Dapazol, from Danish Power Systems ApS, an *m*-PBI membrane, was chosen.[37]

## 2. EXPERIMENTAL SECTION

**2.1. Membrane Materials.** OPBI was purchased from Fumatech BWT GmbH. PVBC was obtained from Scientific Polymer Products. DABCO and 85 wt % *ortho*-PA were purchased from Merck. 1-Azabicyclo(2.2.2)octan-3-ol (quinuclidinol, QOH) and 1-azabicyclo(2.2.2)octane (quinuclidine, Q) were procured from Sigma-Aldrich and Alfa Aesar, respectively. All chemicals were used as received. The Dapazol M40 membrane with a nominal dry thickness of 40 μm was purchased from Danish Power Systems ApS.


https://doi.org/10.1021/acsami.1c17154
ACS Appl. Mater. Interfaces 2021, 13, 56584−56596

**2.2. Membrane Preparation.** 5 wt % OPBI and 15 wt % PVBC solutions were prepared by dissolving the polymers in dimethyl sulfoxide. The OPBI solution was stirred at 50 °C overnight and the PVBC solution for 1 h at rt. Afterward, the solutions were blended to yield weight ratios of OPBI/PVBC of 60:40, 75:25, and 90:10. The blend solutions were stirred for 30 min at room temperature (rt) until homogenization was achieved, followed by casting onto a glass plate. The casting was carried out using an automated film applicator (ZAA 2300, Zehntner) with a blade length of 8 cm and a speed of 20 mm $s^{-1}$. The heights were set to 450, 500, and 630 $\mu$m for the ratios 60:40, 75:25, and 90:10, respectively. The resulting membranes were dried at 80 °C for 24 h, followed by 5 h at 80 °C under reduced pressure. During the 24 h at 80 °C, membranes were covered with a plastic lid to slow down the evaporation rate and achieve cross-linking.[18] The dry thicknesses of all membranes were between 20 and 25 $\mu$m.

The blend membranes were quaternized by immersion in 0.5 M solutions of the three amines (DABCO, quinuclidinol, and quinuclidine) in ethanol for 24 h at 60 °C. Afterward, the membranes were rinsed with DI water.

**2.3. Doping with PA.** Doping was performed by the immersion of membrane pieces of 1 (for weighing), 4 [for ion-exchange capacity (IEC) measurements], or 9 $cm^2$ (for membrane electrode assembly preparation) in 85 wt % aqueous PA at rt. All membranes were doped with PA until saturation was reached (2 days for IPMs and 4 days for Dapazol). PA-doped in-house-prepared membranes had a thickness of 40−50 $\mu$m, and Dapazol had a thickness of 75−80 $\mu$m.

**2.4. Measurement of ADL.** The 1 $cm^2$ membrane pieces were dried at 110 °C and vacuum for 5 h, following the literature,[38] to determine their dry weight ($w_{dry}$). Following, the samples were immersed in 4 mL of aqueous 85 wt % PA until saturation was reached. The drying process was repeated for the doped membrane pieces. This process guaranteed that the weight gain is purely due to PA uptake ($w_{PA}$) and not caused by water uptake. The ADL represents the number of PA molecules per repeating unit of the basic polymer, here OPBI.[39,48] Therefore, eq 1 was used to calculate ADLs

$$\mathrm{ADL} = \frac{w_{PA}}{M_{PA}} \div \frac{w_{dry} \cdot X_{OPBI}}{M_{OPBI}} \tag{1}$$

with the mass fraction of OPBI ($X_{OPBI}$), the molar mass of the repeating unit of OPBI ($M_{OPBI}$), and the molar weight of PA ($M_{PA}$). It should be noted that the interaction of OPBI with PVBC, which forms imidazolium cations (see **2** in Figure 1), is not considered in eq 1.

The membranes' swelling when taking up PA was determined by measuring their $x$, $y$, and $z$ dimensions before and after the doping process using eq 2.[48]

$$\mathrm{Swelling}\ (\%) = 100 \cdot \frac{V_{doped} - V_{undoped}}{V_{undoped}} \tag{2}$$

$V_{doped}$ and $V_{undoped}$ represent the doped and undoped volumes, respectively, calculated by the multiplication of $x$, $y$, and $z$ dimensions for the doped and undoped membrane pieces.

**2.5. Measurement of IEC.** IECs were determined by the back titration method.[40] First, the membranes were conditioned in 0.1 M HCl for 48 h at 90 °C to remove excess amine. Afterward, the membranes were immersed in a 1 M KOH solution at 90 °C for 24 h to exchange $Cl^-$ with $OH^-$. The $OH^-$ form of the membranes was then dried at 110 °C and vacuum for 5 h to determine the dry weight ($w_{dry}$). Afterward, the membranes were immersed in saturated sodium chloride (NaCl) at rt for 24 h. 3 mL of 0.1 M hydrochloric acid (HCl) was added to the saturated NaCl solution, including the membrane, and stirred at rt overnight. The membrane was washed with 25 mL of distilled $H_2O$, which was added to the same solution. This solution was titrated back with a 0.1 M sodium hydroxide (NaOH) solution to determine the remaining HCl using an OMNIS autotitrator (Metrohm Instruments). Equation 3 was used to calculate the IECs.[40]

$$\mathrm{IEC} = \frac{c_{HCl} \cdot V_{HCl} - c_{NaOH} \cdot V_{NaOH}}{w_{dry}} \tag{3}$$

The concentrations of the HCl and NaOH solutions are represented by $c_{HCl}$ and $c_{NaOH}$. $V_{HCl}$ and $V_{NaOH}$ are the used volumes. $W_{dry}$ is the dry weight of the membrane ($OH^-$-form).

The IECs of the in-house-prepared membranes are total IECs, to which the cross-linking points **2** and **3** (see Figure 1) and the imidazole groups of OPBI are contributing.

**2.6. Tensile Testing.** Uniaxial tensile tests were performed on a Shimadzu EZ-SX with a 100 N load cell. The dimensions of the samples were kept constant with 5 cm length and 1.5 cm width. Samples were measured pristine and doped with PA. Young's modulus and elongations at the break were evaluated with stress−strain measurements under ambient conditions with a constant strain rate of 5 mm $min^{-1}$. Young's modulus ($E$) was determined by the stress ($\sigma$) and strain ($\varepsilon$) ratio at a small strain in the linear region (see eq 4).

$$E = \frac{\sigma}{\varepsilon} \tag{4}$$

**2.7. Thermogravimetric Analysis.** Thermogravimetric analysis (TGA) was carried out with samples of approximately 5 mg of the pristine membrane material (before doping with PA) using a TG 209 F1 Libra (NETZSCH). The measurements were carried out under oxidizing (65% $O_2$, 35% $N_2$) conditions to imitate the PA doping and FC measurement atmosphere. The flow rate was set to 40 mL $min^{-1}$ over a temperature range of 30−1000 °C. The samples were loaded into $Al_2O_3$ crucibles.

**2.8. Fabrication of Membrane Electrode Assemblies.** Symmetrical membrane electrode assemblies (MEAs) were fabricated using identical electrodes for the anode and cathode. The ink for the fabrication of gas diffusion electrodes (GDEs) consisted of 1 wt % solid content in a solvent mixture of 50 wt % 2-propanol in water. The solid fraction consisted of 80 wt % Pt/C [Alfa Aesar, 60 wt % platinum (Pt) on carbon] and 20 wt % polytetrafluoroethylene (PTFE) binder (Fuel Cell Store, Teflon Dispersion DISP 30, 60 wt % PTFE). The ink was homogenized using an ultrasonic horn (Hielscher) at 90 W for 30 min at 0 °C. The catalyst ink was deposited onto a Freudenberg H23C8 gas diffusion layer (GDL) via spray coating (ExactaCoat, Sono-Tek). The temperature of the heating stage was set to 90 °C. The ink flow rate was set to 0.33 mL $min^{-1}$ with an ultrasonication power of 5 W, resulting in a deposition rate of approximately 0.03 $mg_{Pt}$ $cm^{-2}$ per deposition cycle until a total Pt loading of 1 mg $cm^{-2}$ was reached. The loading was determined by weighing the GDL and the GDE after the ink deposition. The resulting GDEs were sintered at 360 °C at atmospheric pressure for 20 min (OTF-1200X, MTI Corporation).[41]

For MEA production, the PA-doped membrane was placed between the GDEs and hot-pressed (Carver Inc.) at 150 °C and 10 MPa for 10 min using Pacopads (Pacothane) (3 × 3 $cm^2$) to ensure an equal pressure distribution.[42] Due to the Pacopad dimensions, a total force of 9 kN was applied during hot pressing. The GDEs and hence the resulting active area had dimensions of 2 × 2 $cm^2$ and the membrane had an area of 3 × 3 $cm^2$.

**2.9. Fuel Cell Testing.** FC testing was performed using an 850e FC test system from Scribner Associates Inc. All FCs had an active area of 4 $cm^2$ and were assembled using 150 $\mu$m glass-fiber-reinforced PTFE gaskets on both anode and cathode sides. A GDL compression of approximately 20% was reached when considering the electrodes as noncompressible. A torque of 5 N m was applied to assemble the cell. All tests were run at 180 °C under dry $H_2$ (0.25 L $min^{-1}$) and air (0.75 L $min^{-1}$) at ambient pressure. For conditioning, the FCs were heated up to 120 °C. Following, the $H_2$/air supply was switched on while heating up to 180 °C, and a constant load of 200 mA $cm^{-2}$ was applied until the temperature was reached. Afterward, a constant load of 400 mA $cm^{-2}$ was held for 30 min.[43] The polarization data were measured galvanostatically with a step size of 0.05 A per point in the activation region, 0.2 A in the Ohmic region, and 0.05 A in the mass transport region. The step time was 1 min per point. To evaluate the


https://doi.org/10.1021/acsami.1c17154
ACS Appl. Mater. Interfaces 2021, 13, 56584−56596

Table 1. Initial Peak Power Densities of the Cross-Linked Membranes OPBI-C-PVBC 90−10, 75−25, and 60−40 Quaternized with Quinuclidine, Quinuclidinol, and DABCO[a]

| OPBI:PVBC | quinuclidine | quinuclidinol | DABCO |
|---|---|---|---|
| 90:10 | 246 mW $cm^{-2}$ | **461 ± 11 mW $cm^{-2}$** | 254 mW $cm^{-2}$ |
| 75:25 | 341 mW $cm^{-2}$ | 381 mW $cm^{-2}$ | 362 mW $cm^{-2}$ |
| 60:40 | **529 ± 6 mW $cm^{-2}$** | **529 ± 13 mW $cm^{-2}$** | 372 mW $cm^{-2}$ |

[a]The corresponding polarization and power density curves can be seen in Figure S3. All measurements were carried out at 180 °C under 0.25 L $min^{-1}$ dry $H_2$ at the anode, and 0.75 L $min^{-1}$ air at the cathode, with a Pt loading of 1 mg $cm^{-2}$ at the anode and cathode. The bold values represent the HT-PEMFCs incorporating the best-performing membranes. These measurements were repeated three times, and the initial peak power densities are represented with their standard deviations.

Ohmic cell resistance ($R_\Omega$), the on-line current-interrupt measurement method was used and recorded at each polarization data point.[44]

**2.10. Electrochemical Impedance Spectroscopy.** Electrochemical impedance spectroscopy was carried out using a Scribner 885-HS FC potentiostat (Scriber Associates Inc.). A constant current hold of 15 min was performed at the desired current density (400 and 600 mA $cm^{-2}$) before the measurement. The frequency was swept from 10 kHz to 0.1 Hz with 20 steps per decade. The AC RMS amplitude was set to 10% of the DC current.

**2.11. Linear Sweep Voltammetry.** Linear sweep voltammetry (LSV) was carried out using a Biologic SP-300 potentiostat. Gas flows and cell temperature were controlled using a Scribner 850e (Scribner Associates). The anode was purged with 0.3 L $min^{-1}$ $H_2$ and the cathode with 0.3 L $min^{-1}$ $N_2$ at a cell temperature of 180 °C and atmospheric pressure. The measurements were conducted after polarization data were recorded. Before starting the LSV measurement, the cell was purged with $H_2$ and $N_2$ until the rest potential reached a pseudo-steady-state value. Afterward, the voltage was swept between that steady value and 0.5 V. Higher working electrode potentials were avoided to prevent Pt oxidation. The scan rate was 2 mV $s^{-1}$. The limiting current density was defined after applying a short-circuit correction.[45] Therefore, a linear fit was carried out for the potential window from 0.30−0.40 V. The limiting current density ($j_{H_2\ cross}$) was quantified at 0.3 V. The internal short-circuit resistance (ISR) was estimated from the inverse of the slope of this linear fit.[48]

The hydrogen crossover flux ($\eta_{H_2\ cross}$) was calculated from $j_{H_2\ cross}$ applying Faraday's law according to eq 5

$$\eta_{H_2\ cross} = \frac{j_{H_2\ cross} \cdot A}{n \cdot F} \tag{5}$$

with the FC active area $A$, the number of electrons taking part in the reaction $n$ (here, $2e^-$ per $H_2$ molecule), and the Faraday constant $F$ (96 485 C $mol^{-1}$).[46,47]

**2.12. Inductively Coupled Plasma−Mass Spectrometry.** The phosphorous content of the liquid samples taken from both cell compartments was analyzed by inductively coupled plasma−mass spectrometry (ICP−MS) (PerkinElmer NexION 350x). Samples were prepared as follows: the exhaust gases from the cell passed through 400 mL of distilled water at 10 °C separately at the anode and cathode to collect the exhaust water containing leached PA. Water sampling was carried out after operating the FCs for 48 h at 400 mA $cm^{-2}$. To quantify the phosphorous content, ICP−MS was operated using its dynamic reaction cell (DRC). $O_2$ was used as a DRC cell gas. Instrument parameters were set based on previous literature data (RPa = 0.02 and RPq = 0.40).[48] $^{16}S^{32}O^+$ served as the internal standard. ICP−MS was calibrated daily using a four-point calibration curve. Standards (both the calibration and internal standards) were prepared freshly from stock solutions (Merck Certipur P and S) containing the elements of interest in a given concentration in pure MilliQ water.

## 3. RESULTS AND DISCUSSION

**3.1. OPBI-C-PVBC Membranes.** Figure 1 represents the chemical structure of the cross-linked OPBI with PVBC (OPBI-*c*-PVBC) quaternized with the amines quinuclidine (Q), quinuclidinol (QOH), or DABCO. An $S_N2$-type reaction can occur between the $-CH_2Cl$ moieties of PVBC and the amine group (−NH−) of PBI.[29] Hence, cross-linking probably occurs *via* N-alkylation of the benzimidazole moieties by $-CH_2Cl$ groups (see **1** in Figure 1).[35] Furthermore, the imine moiety in PBI (=N−) can also react with the $-CH_2Cl$ group and form imidazolium cations ($Im^+$) (see **2** in Figure 1) at elevated temperatures,[49−51] which was verified by Lu et al.[35] Postquaternization was carried out by immersing the OPBI-*c*-PVBC membranes into amine solutions in ethanol. An excess of amine was given so that selective quaternization in the case of DABCO was favored, yielding the quaternization of only one nitrogen atom.[35] **3** in Figure 1 represents the quaternizing exemplary with quinuclidine, which is analogous for quinuclidinol and DABCO.

OPBI and PVBC were cross-linked with the ratios 90:10, 75:25, and 60:40. The resulting blends were characterized by attenuated total reflection Fourier-transform infrared (ATR FT-IR) spectroscopy (see Figure S2). For all ratios, the disappearance of the $CH_2-Cl$ bending peak at 1266 $cm^{-1}$ could be observed.[52] Furthermore, the C−N stretching vibration appearing at 1014 $cm^{-1}$ confirmed successful cross-linking.[52] A noticeable stretching vibration of the $-CH_2$ group of PVBC at 2927 $cm^{-1}$ and the C−Cl peak at 692 $cm^{-1}$ loses intensity with the decreasing PVBC content in the blend.[26]

The OPBI-*c*-PVBC membranes were post-treated with three quaternizing agents (DABCO, quinuclidinol, and quinuclidine) and yielded nine membranes. These nine membranes were doped with PA and used as PEMs in HT FC application. The initial peak power densities achieved were compared to each other to evaluate the influence of the blend ratio and/or the quaternizing agent on FC performance.

As can be seen in Table 1, there is one general trend observable for this membrane matrix: the initial peak power density increases with the increasing PVBC content. This can be linked to the increased AU at higher PVBC contents, as shown in Table S1 of the Supporting Information. The AU is, in this context, a better suited measure than the ADL to compare acid contents within the membranes: the ADL calculated from eq 1 will increase when the absolute AU is kept constant if the amount of OPBI in the membrane is reduced. A higher proton conductivity can be expected from 90−10 to 75−25 to 60−40. The only outlier from this trend is the OPBI-*c*-PVBC 90:10 membrane with quinuclidinol. When comparing the effect of different QAs on the maximum peak power density for the maximum amount of PVBC studied in the cross-linked membrane, DABCO shows 44% lower performance compared to quinuclidine and quinuclidinol. DABCO possesses two amine moieties, and both could lead to cross-linking with PVBC. However, when an excess of DABCO is given, presumably, only one nitrogen will undergo cross-


https://doi.org/10.1021/acsami.1c17154
ACS Appl. Mater. Interfaces 2021, 13, 56584−56596

linking.[53] Nevertheless, at this point, we cannot exclude a possible formation of bis-quaternized DABCO, which could lead to a conductivity drop due to the instability of the ammonium groups.[54] Furthermore, Lu et al. reported lower IECs for this type of cross-linked membrane quaternized with DABCO compared to the three best-performing here.[35]

The ratio 60 wt % OPBI to 40 wt % PVBC yielded for quinuclidine and quinuclidinol almost the same initial peak power densities. Therefore, these two membranes were chosen for further analysis to understand the influence of the two different amines, quinuclidine and quinuclidinol, on properties such as swelling, acid doping, mechanical properties, $H_2$ gas crossover, and PA loss during 48 h FC operation. As a third in-house-prepared membrane, the 90 wt % OPBI and 10 wt % PVBC quaternized with quinuclidinol were chosen for further evaluation since it exhibited the third-highest peak power density. This is the only membrane prepared that does not fall into the overall line that the peak power density increases with the increasing PVBC content. At a low PVBC content and, therefore, at low quaternization levels, the OH-moiety could serve as an additional anchor point for the PA network or participate in proton conduction. At a higher PVBC content, with increasing PA uptake, the difference between the membranes quaternized with quinuclidine and quinuclidinol becomes less dominant, probably because now the effect of the amine is the dominant influence compared to the weak interaction of the OH group with PA.

**3.2. Property Comparison of the Three Best-Performing Membranes and a Commercial Membrane.** Membrane properties of the three best-performing OPBI-*c*-PVBC blend membranes (see Table 1) were compared to those of the commercial Dapazol membrane. Therefore, the ADLs, AUs, swelling, IECs, Young's moduli ($E$), elongations at break ($\varepsilon_b$), and tensile strengths at break ($\sigma_E$) were investigated, and the results are shown in Table 2.

The terminology of the quaternized OPBI-*c*-PVBC membranes is [wt % OPBI]-[wt % PVBC]-[abbreviation of amine]. Exemplarily, a blend with 60 wt % OPBI and 40 wt % PVBC quaternized with quinuclidinol will be abbreviated as 60-40-QOH.

We first start by comparing the PA-doping characteristics of the four types of membranes. The achieved ADL for *m*-PBI (Dapazol) of around 13 (see Table 2) is comparable with the ADLs found in the literature for low-molecular-weight *m*-PBI. Yang et al. reported the ADL of intermediate-molecular-weight *m*-PBI to be around 10−11 and of low-molecular-weight *m*-PBI to be about 12−14 when doped in 85 wt % PA at rt.[55,56] The volumetric swelling of around 248 vol % (see Table 2) is also in good accordance with the literature-reported volumetric swelling of *m*-PBI ranging from 150−250 vol %.[1,57] As shown in Table 2, the ADL of 60-40-Q and 60-40-QOH is about 16 and higher than the ADL of *m*-PBI, which is caused by the normalization of the amount of PA absorbed to the amount of PBI in the membrane blends. Therefore, the ADL of 90-10-QOH is also only half of the 60−40 blends. With an absolute AU of around 230% for the 60−40 blends and 180 wt % for the 90-10-QOH membrane, the amount of acid present in the membrane is roughly half of the AU of Dapazol with about 400 wt %. This finding correlates directly with the reduced swelling of the blend membranes with roughly half the value of the commercial Dapazol (see Table 2). The low AU of 90-10-QOH is very promising since the long-term goal in HT-PEMFC development is an HT-PEM without (or less) doping:

**Table 2. ADLs, AU, Swelling, IECs, Young's Moduli (E), Elongations at Break ($\varepsilon_b$), and Tensile Strengths at Break ($\sigma_E$) for the Membranes 60-40-Q, 60-40-QOH, and 90-10-QOH**[a]

| [wt % OPBI-wt % PVBC]-[Amine] | ADL ($mol_{PA}$ $mol_{PBI}^{-1}$) | AU (wt %) | swelling (vol %) | IEC (meq $g^{-1}$) | $E$ (MPa) undoped | $E$ (MPa) doped | $\varepsilon_b$ (%) undoped | $\varepsilon_b$ (%) doped | $\sigma_E$ (MPa) undoped | $\sigma_E$ (MPa) doped |
|---|---|---|---|---|---|---|---|---|---|---|
| 60-40-Q | 16.08 ± 0.19 | 236 ± 3 | 134 ± 3 | 3.14 ± 0.11 | 1684.20 ± 75.37 | 100.87 ± 3.36 | 18.44 ± 1.30 | 25.62 ± 2.14 | 57.75 ± 6.74 | 8.58 ± 1.60 |
| 60-40-QOH | 15.43 ± 0.64 | 227 ± 9 | 130 ± 6 | 3.82 ± 0.23 | 1957.43 ± 67.64 | 135.51 ± 12.13 | 11.78 ± 0.17 | 23.82 ± 3.11 | 74.99 ± 5.05 | 10.10 ± 1.71 |
| 90-10-QOH | 8.05 ± 0.16 | 177 ± 4 | 130 ± 1 | 3.94 ± 0.05 | 2656.44 ± 39.61 | 262.76 ± 31.94 | 14.15 ± 2.82 | 44.35 ± 2.53 | 107.81 ± 9.62 | 22.27 ± 0.31 |
| Dapazol | 12.70 ± 0.89 | 404 ± 28 | 248 ± 10 | 6.49[b] | 2738.09 ± 68.53 | 87.20 ± 4.15 | 40.45 ± 3.09 | 139.78 ± 5.33 | 110.88 ± 3.27 | 14.77 ± 2.16 |

[a]Young's moduli ($E$), elongations at break ($\varepsilon_b$), and tensile strength values at break ($\sigma_E$) are shown for doped and undoped samples at rt. The values are the mean of three replicates and are represented with their standard deviations. It should be noted that the cross-linking points **2** and **3** and the imidazole moieties of OPBI are contributing to the IECs of the in-house-prepared membranes. [b]Theoretically calculated (see the Supporting Information).



https://doi.org/10.1021/acsami.1c17154
ACS Appl. Mater. Interfaces 2021, 13, 56584−56596

the PA is the limiting factor due to its evaporation and leaching during FC operation. Nonetheless, as shown in Table 1, 90-10-QOH within an HT-PEMFC showed a slightly lower initial peak power density than 60-40-Q and 60-40-QOH, indicating that the lower PA content in this membrane may pose a limiting factor for its performance.

It is known that cross-linking enhances the mechanical properties of membranes, reduces softening and volumetric swelling with the increasing PA content, and allows for higher ADLs. Generally, higher AUs while maintaining mechanical stability are desirable since high AUs are expected to lead to higher proton conductivities.[58] The same behavior can be observed for $F_6$PBI. Li et al. reported an ADL of 7 for pure $F_6$PBI when doped in 75 wt % PA at rt for 100 h,[59] while blends with $F_6$PBI showed higher ADLs. In an earlier study, we have reported an ADL of 10 for a blend membrane of $F_6$PBI and PWN [phosphonated poly(pentafluorostyrene)][39] and Yang et al. reported an ADL of around 14 for a blend of $F_6$PBI and chloromethyl polysulfone when doped at rt in 85 wt % PA for 120 h.[27] There are two possible reasons for achieving higher ADLs when using OPBI and quaternization instead of $F_6$PBI. First, the more flexible structure of OPBI can increase the number of incorporated free PA molecules within the polymer matrix. Second, two cationic groups (quaternized amine and imidazolium, **3** and **2** in Figure 1) can stabilize the anions of PA and hence increase proton concentration within the membrane compared to a pure PBI membrane.

All membranes prepared in this work showed high IECs ranging from 3 to 4 meq $g^{-1}$ (see Table 2). This is in agreement with the literature. Lu et al. reported for this type of cross-linked membrane an IEC of 2.51 meq $g^{-1}$ for PBI-*c*-PVBC with DABCO as a quaternizing agent.[35] Kulkarni et al. reported an IEC of 2.95 meq $g^{-1}$ for sulfone-substituted OPBI and of 4.2 meq $g^{-1}$ for postsulfonated OPBI (sOPBI).[60] Since Dapazol is a pure PBI membrane, the IEC was calculated to be 6.49 meq $g^{-1}$ (see the Supporting Information). As shown in Table 2, the IECs of the membranes 90-10-QOH and 60-40-QOH showed almost equal values.

The amount of PA in the membrane is important for the ionic conductivity during HT-PEMFC operation, and it also largely influences the mechanical properties. Thus, stress−strain tests were executed with the pristine and doped membrane samples. With a Young's modulus of around 2700 MPa, undoped Dapazol shows the highest rigidity, closely followed by the undoped 90-10-QOH membrane. This is in agreement with the literature. Zhang et al. reported an elastic modulus of 2950 MPa for OPBI.[61] As the mechanical stability in the polymer blends stems predominantly from the OPBI chain, a strong decrease in Young's moduli for the 60−40 blends is expected.[35] After PA doping, however, Dapazol loses most of its mechanical stability, and the Young's modulus is dropping to only 3% of its value in the undoped state. As the commercial membrane is not cross-linked, the PA uptake results in a strong softening effect as the chains can now very easily slide off from each other. The Young's moduli of the cross-linked 60−40 membrane blends also drop significantly to 6−7% of their undoped values, resulting in a higher Young's modulus in the doped state compared to Dapazol. Both the reduced AU and the cross-linking could explain the higher maintenance of stability upon doping. Of special interest is the 90-10-QOH membrane as it keeps almost 10% of its high Young's modulus in the completely doped state, therewith significantly outperforming the other membranes and resulting in a doped Young's modulus 3 times higher compared to Dapazol. The tensile strengths at break ($\sigma_E$) of undoped 90-10-QOH and Dapazol are almost the same with 108−111 MPa. Zhang et al. reported a tensile strength of 129.5 MPa for undoped OPBI.[61] The tensile strength of undoped 90-10-QOH is in accordance with the literature when considering the 90 wt % OPBI in the membrane. Yang et al. reported a tensile strength of 116.8 MPa for an undoped *m*-PBI membrane.[27] Hence, the tensile strength of Dapazol is 110.88 MPa, in good accordance with the literature (see Table 2). 60-40-QOH and 60-40-Q exhibit lower tensile strengths of 74.99 and 57.75 MPa, respectively, presumably due to the lower OPBI content within the membrane. The tensile strength at break after doping is lower for all membranes due to the plasticizing effect of PA.[55] Dapazol with a tensile strength of 14.77 MPa at rt and an ADL of 12.70 is in accordance with the literature.[27,55] 90-10-QOH shows the highest tensile strength of 22.27 MPa after doping with PA due to its lower AU of less than 200 wt % compared to the other membranes (see Table 2). Furthermore, it can be seen that the elongations at break for Dapazol are significantly higher than those for the blend membranes, in both the doped and undoped states (see Table 2). Higher elongations at break of pure PBI compared to those of the blend membranes can be explained by the lack of cross-links within this membrane, which allows this polymer to stretch without breaking covalent bonds. In general, the elongations at break were larger when doped compared to the undoped state of the membranes. This finding can be attributed to the plasticizing effect of absorbed PA.[55] For the OPBI-*c*-PVBC membranes, the increase in elongations at break upon doping was around 2−3 times, which is lower than that for Dapazol, which exhibited an increase of 3.5 times. This result confirms the better mechanical properties of the OPBI-*c*-PVBC membranes and correlates with both the higher AU and the higher volumetric swelling of Dapazol compared to those of the blend membranes.

The thermal-oxidative stability of the PEMs was investigated in oxygen-enriched synthetic air (65% $O_2$ and 35% $N_2$) by TGA (see Figure 2). The mass loss until 100 °C is due to water evaporation. Both PBI-types, *m*-PBI and OPBI, exhibited a high thermal-oxidative stability up to 400 °C. The cross-linked membranes showed thermal-oxidative stabilities up to 260 °C, where mass losses due to the degradation of PVBC can be observed. Within this range also mass losses due to the amines occur. The membrane 90-10-QOH containing 90 wt % OPBI showed a mass loss of around 10% between 260 and 480 °C due to the full loss of PVBC. The membranes containing 60 wt % OPBI exhibited lower thermal-oxidative stability due to their higher PVBC content. In general, all membranes exhibited high thermal-oxidative stabilities, verifying that PEMFC operation at 180 °C poses no thermal limit for the blend membranes.

Furthermore, the membranes 60-40-Q, 60-40-QOH, and 90-10-QOH revealed an amorphous nature as verified by X-ray diffraction (see Figure S6). Additionally, Fenton's test was carried out to investigate the oxidative stability of the membranes 60-40-Q, 60-40-QOH, 90-10-QOH, and Dapazol. The corresponding data can be found in the Supporting Information (Figure S7).

**3.3. Fuel Cell Characterization.** The polarization and power density curves for the HT-PEMFCs incorporating the PA-doped membranes prepared in this work as well as the commercial Dapazol are shown in Figure 3.



https://doi.org/10.1021/acsami.1c17154
ACS Appl. Mater. Interfaces 2021, 13, 56584−56596

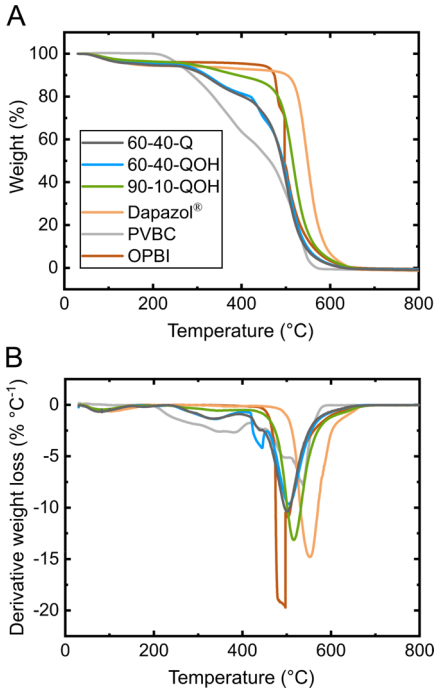


**Figure 2.** (A) TGA and (B) derivative of the TGA data for the membranes 60-40-Q, 60-40-QOH, 90-10-QOH, its blend components OPBI and PVBC, and the commercial Dapazol membrane under oxidative conditions (65% $O_2$ and 35% $N_2$).

It can be seen that the OPBI-*c*-PVBC incorporating FCs outperformed the FC with Dapazol (see Figure 3). The FCs with 60-40-Q and 60-40-QOH perform almost identically with an initial peak power density of 529 mW $cm^{-2}$ at 1550 mA $cm^{-2}$ (see Table 3). 90-10-QOH shows an initial peak power density of 461 mW $cm^{-2}$ at a current density of 1440 mA $cm^{-2}$. Dapazol shows the lowest initial peak power density with 424 mW $cm^{-2}$ at 1210 mA $cm^{-2}$ (see Figure 3B). FCs incorporating PA-doped Dapazol showed lower reproducibility, especially in the mass transport region at >1000 mA $cm^{-2}$ (see Figure 3A). We assume that the poor reproducibility in the mass transport region was due to the weaker mechanical properties of the commercial membrane, such as increased swelling, which possibly leads to a blocking of the catalyst layer pores, hindering the transport of fuel, oxidant, and product water.

At low current densities (below 100 mA $cm^{-2}$), all polarization curves show a similar behavior. This result is in agreement with the usage of equal electrodes for all MEAs, irrespective of the membrane type. It should be noted that polarization data were recorded after a holding time of 30 min at 400 mA $cm^{-2}$. Following the literature, the break-in process is considered to be around 48 to 100 h.[62] Hot-pressing is known to reduce the break-in time since it enhances the transfer of free PA from the doped PEM to the catalyst layer.[1] Initial polarization data were recorded after 30 min at 180 °C and 400 mA $cm^{-2}$, as the data showed high reproducibility (compare Figure 3), while for PA loss, a 48 h constant current hold at 400 mA $cm^{-2}$ was carried out.

To understand the influence of the PEM on FC performance, the Ohmic region was analyzed in more detail. Therefore, we investigated the HFRs and fuel inefficiency caused by fuel crossover. Impedance measurements were carried out at 400 and 600 mA $cm^{-2}$ for each of the three replicates. The mean HFR and its standard deviations are shown in Table 3. The HFRs ranged between 88 and 104 mΩ $cm^2$. 90-10-QOH and Dapazol showed almost the same HFRs, which are slightly

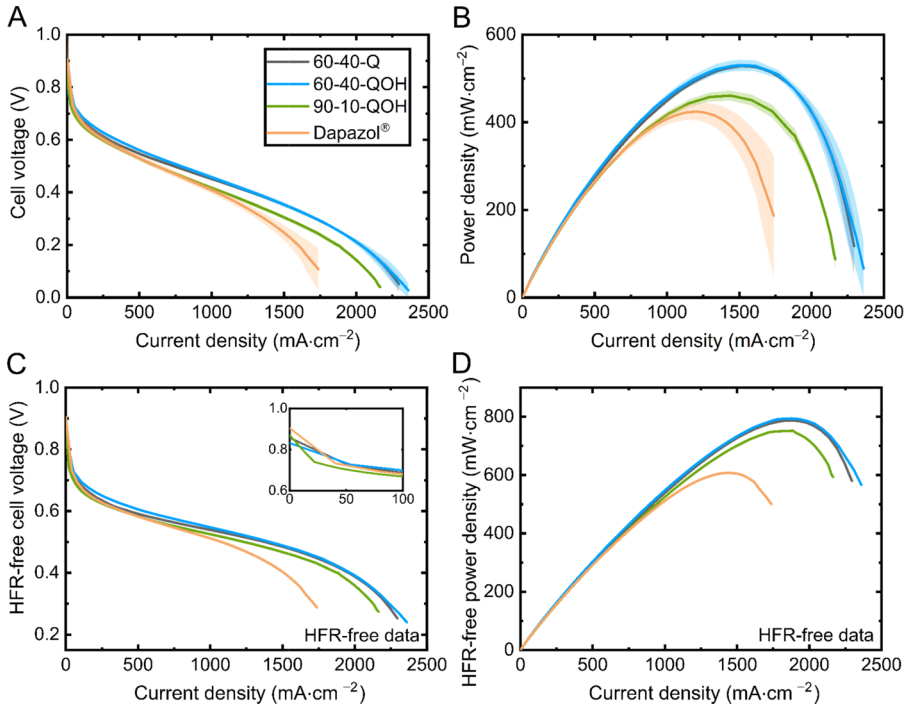


**Figure 3.** Initial polarization and power density curves for the FCs based on the membranes 60-40-Q, 60-40-QOH, 90-10-QOH, and Dapazol. All measurements were carried out at 180 °C under 0.25 L $min^{-1}$ dry $H_2$ at the anode and 0.75 L $min^{-1}$ air at the cathode, with a Pt loading of 1 mg $cm^{-2}$ at the cathode and anode. Each curve in (A,B) represents the mean of three measurements of three different MEAs. The shaded areas represent standard deviations. In (C,D), the high-frequency resistance (HFR)-free data of the mean of the three FC measurements are represented.


https://doi.org/10.1021/acsami.1c17154
ACS Appl. Mater. Interfaces 2021, 13, 56584−56596

Table 3. OCV Values and Initial Peak Power Densities for Figure 3A with Their Standard Deviations of Three Replicates[a]

| wt % [OPBI-wt % PVBC]-[Amine] | OCV (V) | peak power density (mW cm$^{-2}$) | HFR (mΩ cm$^2$) | $\sigma$ (mS cm$^{-1}$) |
|---|---|---|---|---|
| 60-40-Q | 0.83 ± 0.11 | 529 ± 6 | 87.76 ± 9.80 | 92.16 ± 17.17 |
| 60-40-QOH | 0.83 ± 0.06 | 529 ± 13 | 90.29 ± 5.12 | 85.42 ± 8.22 |
| 90-10-QOH | 0.87 ± 0.08 | 461 ± 11 | 107.58 ± 9.29 | 65.04 ± 8.99 |
| Dapazol | 0.90 ± 0.12 | 424 ± 20 | 104.36 ± 8.49 | 120.94 ± 15.64 |

[a]HFR values were defined as the mean of six measurements (from impedance data at 400 and 600 mA cm$^{-2}$, each three measurements). Membrane conductivities ($\sigma$) are derived from HFR values and correction for the electronic resistances. Here, the conductivities at 180 °C are given. A more detailed explanation and conductivities at 140 and 160 °C can be found in the Supporting Information (Figure S5).

higher than those for 60-40-Q and 60-40-QOH (see Table 3). The HFR is dependent on the AU and the membrane thickness, which explains the order with respect to the HFR of 60-40-Q ≈ 60−40QOH < 90-10-QOH ≈ Dapazol. Generally, it can be noted that the different performances of the FCs correlate with their HFRs and, therefore, with Ohmic resistances of the membranes, as can also be seen in the HFR-corrected polarization and power density plots in Figure 3C,D. When excluding contributions from the HFR, the performance of the MEAS with IPMs still outperforms the one with Dapazol, especially at high current densities. This phenomenon is most likely due to the almost 2 times higher volumetric swelling behavior of Dapazol when doped with PA compared to that of the in-house-prepared PEMs (see Table 2). While Dapazol, despite its increase in thickness, still shows a comparable HFR to the IPMs, excessive swelling presumably leads to characteristic mass transport-restricted voltage losses for potentials below 0.4 V (see Figure 3A).

Fuel crossover is an important parameter for membrane materials in FC application. Therefore, we carried out LSV to detect $H_2$ gas crossover on one replicate per membrane type. The LSV data are represented in Figure 4A. Ideally, the current response follows a saturation curve, of which the maximum corresponds to the hydrogen crossover. However, the expected curvature at around 0.2 V is followed by a linear increase of the current density. This saturation regime is the sum of the hydrogen crossover and a superimposed short-circuit component.[63] The latter occurs with increased potential of the working electrode due to an electrical short across the PEM. Figure 4B represents the short-circuit-corrected linear sweep voltammograms (see Figure S4 for an exemplary short-circuit correction).

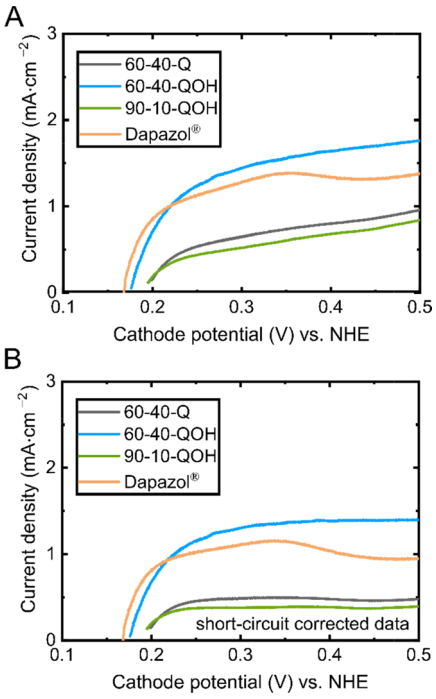


Figure 4. (A) Linear sweep voltammograms and (B) linear sweep voltammograms with internal short-circuit correction. All measurements were carried out at 180 °C, with 0.3 L min$^{-1}$ dry $H_2$ at the anode and 0.3 L min$^{-1}$ $N_2$ at the cathode with a scan rate of 2 mV s$^{-1}$.

LSV was carried out on one replicate, and the corresponding values can be found in Table 4. The cells used for LSV characterization showed OCVs of 0.94 (60-40-Q), 0.86 (60-40-QOH), 0.95 (90-10-QOH), and 0.93 V (Dapazol). 60-40-QOH showed the highest hydrogen crossover with 2.88 × 10$^{-11}$ mol s$^{-1}$. The lowest gas crossover was observed for 90-10-QOH with 7.26 × 10$^{-12}$ mol s$^{-1}$, which is almost 3 times smaller than the gas crossover of Dapazol (see Table 4). The OCVs are in accordance with the hydrogen gas crossover fluxes shown in Table 4. 90-10-QOH with the lowest hydrogen gas crossover exhibited the highest OCV. Just as the HFR, the $H_2$ crossover is also dependent on the thickness of the membrane. Furthermore, the polymer ratio and the degree of cross-linking may have an influence. Minding the variation in OCV observed for replicates of the same PEMs (see Table 3), we do not want to put an emphasis on the exact values obtained by the $H_2$ crossover LSV analysis. It is important, however, to stress that IPMs can obtain lower crossover rates and similar ISRs at lower absolute thicknesses compared to the commercial Dapazol membrane. As the casting process is not close to any commercial scale yet, the variance is not addressed in more detail here.

Furthermore, hydrogen gas crossover depends on operating conditions, such as temperature and gas pressure.[64] All the obtained limiting current densities here are in good agreement with the literature and show even lower hydrogen permeations at a higher operating temperature (180 °C). Galbiati et al. reported for the BASF Celtec-P2100 MEA with an active area of 20 cm$^2$ limiting current densities between 0.5 and 13.8 mA cm$^{-2}$ for FC operation at 160 °C.[63] Pinar et al. reported for the Celtec-P1100W MEA with an active area of 20.25 cm$^2$ a permeation flux of 2.46 × 10$^{-7}$ mol s$^{-1}$ for a FC operation temperature of 160 °C.[62]

By the inverse of the slope of the linear region (see Figure 4A), the ISR can be evaluated. 60-40-Q exhibited with 625 Ω cm$^2$, the lowest ISR (see Table 4) followed by Dapazol. 90-10-QOH showed the highest ISR of 906 Ω cm$^2$. This finding is noteworthy since Dapazol exceeds the thickness of the OPBI-*c*-PVBC membranes, which would, for a constant membrane material, typically result in a higher ISR. The fact that Dapazol shows a lower ISR than 90-10-QOH can be correlated with the worse mechanical properties, such as high swelling and low


https://doi.org/10.1021/acsami.1c17154
ACS Appl. Mater. Interfaces 2021, 13, 56584−56596

Table 4. Limiting Current Density $j_{H_2\ cross}$, Hydrogen Crossover Flux ($\eta_{H_2\ cross}$), and Internal Short-Circuit Resistances (ISRs) for Single-Cell Measurements[a]

| [wt % OPBI-wt % PVBC]-[Amine] | $j_{H_2\ cross}$ (mA cm$^{-2}$) | $\eta_{H_2\ cross}$ (mol s$^{-1}$) | ISR (Ω cm$^2$) | OCV (V) |
|---|---|---|---|---|
| 60-40-Q | 0.49 | $1.01 \times 10^{-11}$ | 625 | 0.94 |
| 60-40-QOH | 1.39 | $2.88 \times 10^{-11}$ | 899 | 0.86 |
| 90-10-QOH | 0.35 | $7.26 \times 10^{-12}$ | 906 | 0.95 |
| Dapazol | 0.95 | $1.98 \times 10^{-11}$ | 769 | 0.93 |

[a]ISRs represent the inverse of the slopes between 0.30 and 0.40 V for the IPMs and between 0.45 and 0.50 V for Dapazol of the linear sweep voltammograms (Figure 4A). Furthermore, the OCVs of the FCs used for LSV characterization are shown. The OCVs were taken from polarization data recorded after a 30 min hold at 400 mA cm$^{-2}$ at 180 °C under 0.25 L min$^{-1}$ $H_2$ and 0.75 L min$^{-1}$ air before LSV measurements.

Young's modulus of the commercial membrane. Again, due to variances in membrane casting, emphasis should not be put on exact values but on the overall possibility of improving the ISR by use of IPMs in HT-PEMFCs.

**3.4. PA Loss over Time.** For PA loss monitoring, high flow rates (0.25 L min$^{-1}$ $H_2$, 0.75 L min$^{-1}$ air, and $\lambda_{H_2}/\lambda_{air}$ = 9/11) and an operating temperature of 180 °C were chosen. A constant current density of 400 mA cm$^{-2}$ was held for 48 h, and the voltage profiles over time are shown in Figure 5. The amount of PA in the collected samples was quantified by ICP–MS.

As can be seen, all FCs showed a similar degradation behavior approximately within the first 20 h (see Figure 5A). Since the electrodes were kept the same for all measurements, a similar behavior regarding degradation was to be expected. Degradation reasons within this time frame are presumably caused by poisoning of the Pt catalyst by PA. The initially sharper drop in the voltage of the cell with Dapazol compared to the other cells can be explained by its higher AU (see Table 2) and its presumably deeper extension into the catalyst layer. Dapazol might thus poison the catalyst more strongly and more quickly than the other membranes. After a specific saturation is reached, the following continuous voltage decay can be assumed to correlate with the PA loss leading to lower conductivities.

For the further understanding of FC degradation, the cell resistances were investigated by the current interrupt method (see Figure 5B). Within the first up to 30 h, all cells showed a decrease in cell resistance, which indicates that the break-in of the cells was not completed yet. Hence, only the last 18 h were considered for further evaluation. The voltage decays and cell resistance increases for the last 18 h are listed in Table 5. There is an inverse correlation between a higher increase in cell resistance (see Table 5) and the AU of the PEMs (see Table 2). The FC with Dapazol, which exhibited an almost 2 times higher AU compared to the IPMs, showed the lowest increase of cell resistance. The more acid present in the membrane, the less vulnerable it will most likely be for the resistance to increase strongly upon the removal of small amounts of acid. In agreement with this, the IPM with the lowest AU, 90-10-QOH, exhibited the largest increase in cell resistance. The resistance increase of the 60–40 blends is rather similar and lies between the increase of the Dapazol and the 90-10-QOH IPM. Along with the increased cell resistance, the voltage decays. Also, here, the Dapazol membrane behaves most stable.

The change in cell resistance throughout this constant current hold is seen to arise from a change in the Ohmic resistance of the membrane caused by acid removal. The Ohmic resistance is predominantly influenced by the PA content, which itself is a simple function of the acid level after

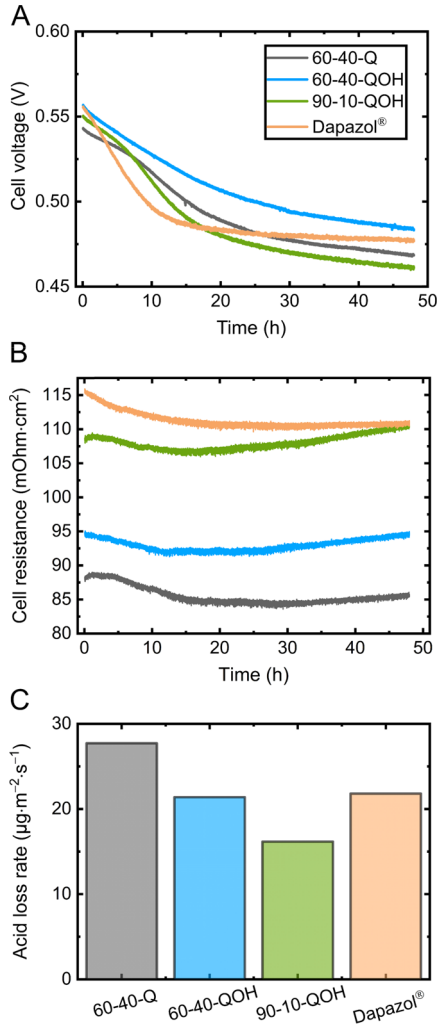


Figure 5. (A) Cell voltage over time for 48 h at 400 mA cm$^{-2}$ with 0.25 L min$^{-1}$ $H_2$ and 0.75 L min$^{-1}$ air at 180 °C, (B) corresponding cell resistance by current interruption, and (C) cathodic area-specific acid loss rates during 48 h at 400 mA cm$^{-2}$.

doping and the removal of PA over time. The amounts of PA found in the cathode exhaust water are shown in Figure 5C and Table 5. It should be noted that over 120 °C PA, dimerization occurs, leading to the formation of pyrophosphoric acid ($H_4P_2O_7$) and water production. This will lead to an increase in membrane conductivity due to elevated temperatures and an increase in resistance due to PA dimerization[65]

Even though the cell with the Dapazol membrane shows the most stable performance over time, it is not the one with the


https://doi.org/10.1021/acsami.1c17154
ACS Appl. Mater. Interfaces 2021, 13, 56584–56596

Table 5. Voltage Decay and Increase of Cell Resistance during Fuel Cell Operation, Cathodic Acid Loss Rate, and Total Phosphorus Losses for the Cathode and Anode[a]

| [wt % OPBI-wt % PVBC]-[Amine] | voltage decay ($\mu V \cdot h^{-1}$) | increase of cell resistance ($m\Omega \cdot cm^2 \cdot h^{-1}$) | cathodic acid loss rate ($\mu g \cdot m^{-2} \cdot s^{-1}$) | cathodic total P loss ($\mu g$) | anodic total P loss ($\mu g$) |
|---|---|---|---|---|---|
| 60-40-Q | −479 | 0.07 | 27.71 | 605 | 5.11 |
| 60-40-QOH | −556 | 0.10 | 21.39 | 467 | -[b] |
| 90-10-QOH | −490 | 0.16 | 16.17 | 353 | -[b] |
| Dapazol | −154 | 0.02 | 21.80 | 476 | -[b] |

[a]Voltage decay and cell resistance increase rates were defined for the time range from 30 to 48 h. The acid loss rate was calculated for a total of 48 h. [b]Untraceable. The limit of detection for *P* was 5 $\mu g\ L^{-1}$.

lowest but with the second largest PA loss. Due to the high amount of PA present in the membrane at the begin-of-test, however, this acid loss does not impair the steady-state performance significantly. Even though the constant current hold of the two 60−40 IPM blends showed similar stability values, the amount of PA leached in the case of 60-40-Q is almost 30% higher than the amount found in the exhaust of the 60-40-QOH cell. This can be explained by the main difference in their chemical structure: the OH-functionality of the amine quinuclidinol (see Figure 1). It may help to stabilize PA within the membrane since it is an additional anchor point to retain PA molecules through hydrogen bridging. The membrane with the lowest AU, 90-10-QOH, showed the highest resistance increase throughout the constant current hold. The absolute amount of PA found in the exhaust is, however, the lowest. This is seen to be a combination of both the higher affinity of the quniuclidinole QA to retain PA and the overall lower amount of PA present in the membrane at the begin-of-test. Considering the mass of PA for 4 $cm^2$ membrane pieces, 60-40-Q loses 8.92%, 60-40-QOH 4.81%, 90-10-QOH 4.88%, and Dapazol 1.92% of PA (see Table S2). This confirms that the OH functionality may help to stabilize PA within the membrane since both 60-40-QOH and 90-10-QOH show an almost identical PA loss.

Søndergaard et al. showed that the acid loss is dependent on temperature, flow rate, and current density.[66] The reported acid loss rates for a total flow rate of 1 L $min^{-1}$ (air + $H_2$) at 180 °C are 17 $\mu g\ m^{-2}\ s^{-1}$ at 200 mA $cm^{-2}$, 48 $\mu g\ m^{-2}\ s^{-1}$ at 600 mA $cm^{-2}$, and 59 $\mu g\ m^{-2}\ s^{-1}$ at 800 mA $cm^{-2}$. We detected acid loss rates between 16.17 and 27.71 $\mu g\ m^{-2}\ s^{-1}$ (see Table 5) for the same total flow rate but at 400 mA $cm^{-2}$, which are in agreement with the literature. One main difference between the study of Søndergaard et al. and this study was FC operation time periods. Søndergaard et al. operated FC measurements for 42 000 h, while only operation times of 48 h were investigated in this work. Nonetheless, acid loss rates have been suggested to be lower after long-term operation compared to shorter periods of time.[67]

Interestingly, the anodic PA loss was very low or untraceable compared to the cathodic PA loss (see Table 5). Anodic P losses were either untraceable or a maximum of 5.11 $\mu g$. Becker et al. described in 2018 that PA anions migrate from the cathode to the anode and recombine with protons to PA.[68] This migration causes a concentration gradient, which in turn causes back diffusion of acid from the anode to the cathode but still favors acid loss on the cathode side. This explanation is in agreement with our results. It should be noted that the PA back diffusion rate will be more limiting at larger current densities. Furthermore, Kannan et al. reported a 2 times higher acid loss at the cathode exhaust compared to that at the anode with 1 order of magnitude higher cathode exit flow.[69]

## 4. CONCLUSIONS

This study evaluated the properties and FC performances of cross-linked OPBI and PVBC membranes after decoration with QA groups from three different amines and doping with PA. FC tests revealed that quinuclidine and quinuclidinol resulted in higher power densities than DABCO. This result is interesting since DABCO is a more frequently used quaternizing agent, especially in the field of anion-exchange membranes. The best PEMs for FC application were the membranes with OPBI to PVBC ratios of 90:10 quaternized with quinuclidinol, 60:40 quaternized with quinuclidinol, and 60:40 quaternized with quinuclidine. All three membranes outperformed the PA-doped commercial Dapazol, with the last two showing the highest and almost identical initial peak power densities and the highest current density output when operated within an HT-PEMFC (530 mW $cm^{-2}$ at 1550 mA $cm^{-2}$ under $H_2$/air operation at 180 °C and ambient pressure). The reproducibility of the FC resulting at high current densities was superior compared to that of the commercial Dapazol, which can be explained by the poor mechanical properties of Dapazol, upon doping with PA. With an AU of 404 wt %, Dapazol showed the lowest FC performance with an initial peak power density of 424 mW $cm^{-2}$ at 1210 mA $cm^{-2}$, while the membranes OPBI to PVBC 60:40 quaternized with quinuclidine and quinuclidinol showed AUs of roughly 230 wt %. With the membrane 90 wt % OPBI and 10 wt % PVBC quaternized with quinuclidinol, an initial peak power density of 461 mW $cm^{-2}$ at 1440 mA $cm^{-2}$ was achieved. The lower power density can be explained by its lower AU of 177 wt %, which resulted in larger Ohmic losses.

While the Ohmic contribution of Dapazol-based MEAs was roughly comparable to that of the MEAs with IPMs, the Dapazol-based MEAs suffered from an earlier onset of mass transport-related losses, which explain their limited peak power density. Thus, it can be concluded that the higher AU of Dapazol enabled this membrane to maintain an almost equal proton conductivity as the IPMs, despite its larger thickness, however, at the cost of poor mechanical properties, which can explain its pronounced mass transport resistance. The investigated IPMs offered superior mechanical properties at lower thicknesses, which allowed these membranes to provide a very reproducible FC performance and a hydrogen crossover that is comparable to Dapazol.

Regarding PA leaching, all membranes showed amounts of P in the off-gas analysis in the same order of magnitude. Due to the higher AU during doping, the acid content loss of the Dapazol membrane over 48 h is 1.92% less than that of the IPMs, resulting in a more stable electrochemical performance. It could be observed that the membranes quaternized with quinuclidinol (4.81−4.88% PA loss) showed better PA retention compared to the membrane quaternized with


https://doi.org/10.1021/acsami.1c17154
ACS Appl. Mater. Interfaces 2021, 13, 56584−56596

quinuclidine (8.92% PA loss). The additional −OH group of quinuclidinol compared to that of quinuclidine is a possible explanation for this finding, as the polar moiety may improve acid retention.

Taken together, we have found that PA/OPBI-*c*-PVBC decorated with QA groups is a very promising membrane system for HT-PEMFCs. The results indicate that it offers higher peak FC performances compared to commercial HT-PEMs. It requires a relatively small total PA uptake and shows high mechanical stability at low thicknesses. However, its low initial PA content also makes it more susceptible to acid loss compared to a membrane with a higher total AU. In order to obtain mechanically stable, low-acid, and long-term stable membranes, the acid retention capacity of IPMs with QA groups has to be addressed in the future work. Furthermore, the OPBI-*c*-PVBC membrane systems could be quaternized with different amines such as trimethylamine to have a better understanding of the influence of the used quaternizing agent on FC performance and acid retention.

## ■ ASSOCIATED CONTENT

### Supporting Information

The Supporting Information is available free of charge at https://pubs.acs.org/doi/10.1021/acsami.1c17154.

Chemical structures and molar masses of $F_6$PBI, OPBI, *m*-PBI, and PVBC; ATR FT-IR spectra of the polymers OPBI and PVBC and the cross-linked membranes; polarization and power density curves for the FCs in Table 1; ADLs and AUs for all membranes discussed in this work; PA uptake in milligram, cathodic P and PA losses, and acid loss; exemplary short-circuit correction for the linear sweep voltammogram of 90-10-QOH; *in situ* proton conductivities at 140, 160, and 180 °C; XRD spectra; and Fenton's test (PDF)

## ■ AUTHOR INFORMATION


### Corresponding Authors

**Funda Arslan** − *Forschungszentrum Jülich GmbH, Helmholtz Institute Erlangen-Nürnberg for Renewable Energy (IEK-11), 91058 Erlangen, Germany; Department of Chemical and Biological Engineering, Friedrich-Alexander-Universität Erlangen-Nürnberg, 91058 Erlangen, Germany;* orcid.org/0000-0001-5273-192X; Email: f.arslan@fz-juelich.de

**Thomas Böhm** − *Forschungszentrum Jülich GmbH, Helmholtz Institute Erlangen-Nürnberg for Renewable Energy (IEK-11), 91058 Erlangen, Germany;* orcid.org/0000-0003-2036-2159; Email: t.boehm@fz-juelich.de

### Authors

**Khajidkhand Chuluunbandi** − *Forschungszentrum Jülich GmbH, Helmholtz Institute Erlangen-Nürnberg for Renewable Energy (IEK-11), 91058 Erlangen, Germany; Department of Chemical and Biological Engineering, Friedrich-Alexander-Universität Erlangen-Nürnberg, 91058 Erlangen, Germany*

**Anna T.S. Freiberg** − *Forschungszentrum Jülich GmbH, Helmholtz Institute Erlangen-Nürnberg for Renewable Energy (IEK-11), 91058 Erlangen, Germany; Department of Chemical and Biological Engineering, Friedrich-Alexander-Universität Erlangen-Nürnberg, 91058 Erlangen, Germany;* orcid.org/0000-0002-7885-7632

**Attila Kormanyos** − *Forschungszentrum Jülich GmbH, Helmholtz Institute Erlangen-Nürnberg for Renewable Energy (IEK-11), 91058 Erlangen, Germany;* orcid.org/0000-0002-2145-7419

**Ferit Sit** − *Forschungszentrum Jülich GmbH, Helmholtz Institute Erlangen-Nürnberg for Renewable Energy (IEK-11), 91058 Erlangen, Germany*

**Serhiy Cherevko** − *Forschungszentrum Jülich GmbH, Helmholtz Institute Erlangen-Nürnberg for Renewable Energy (IEK-11), 91058 Erlangen, Germany;* orcid.org/0000-0002-7188-4857

**Jochen Kerres** − *Forschungszentrum Jülich GmbH, Helmholtz Institute Erlangen-Nürnberg for Renewable Energy (IEK-11), 91058 Erlangen, Germany; Faculty of Natural Science, North-West University, Potchefstroom 2520, South Africa*

**Simon Thiele** − *Forschungszentrum Jülich GmbH, Helmholtz Institute Erlangen-Nürnberg for Renewable Energy (IEK-11), 91058 Erlangen, Germany; Department of Chemical and Biological Engineering, Friedrich-Alexander-Universität Erlangen-Nürnberg, 91058 Erlangen, Germany;* orcid.org/0000-0002-4248-2752

Complete contact information is available at: https://pubs.acs.org/10.1021/acsami.1c17154


### Notes

The authors declare no competing financial interest.

## ■ ACKNOWLEDGMENTS

We thank Dillam Diaz Romero and Julian Stonawski for helpful discussions. We also gratefully thank the Bavarian Ministry of Economic Affairs, Regional Development and Energy through the project "Emissionsfreier und stark emissionsreduzierter Bahnverkehr auf nicht-elektrifizierten Strecken" for the financial support, which made this work possible. Furthermore, we thank Marco Sarcletti and Andreas Eigen from the Institute of Polymer Materials at the Friedrich-Alexander University Erlangen-Nürnberg for introduction to and usage of the instrument for TGA measurements.

## ■ REFERENCES

(1) Aili, D.; Henkensmeier, D.; Martin, S.; Singh, B.; Hu, Y.; Jensen, J. O.; Cleemann, L. N.; Li, Q. Polybenzimidazole-Based High-Temperature Polymer Electrolyte Membrane Fuel Cells: New Insights and Recent Progress. *Electrochem. Energy Rev.* **2020**, *3*, 793.

(2) von Helmolt, R.; Eberle, U. Fuel Cell Vehicles: Status 2007. *J. Power Sources* **2007**, *165*, 833−843.

(3) Zhu, Y.; Zhu, W. H.; Tatarchuk, B. J. Performance Comparison between High Temperature and Traditional Proton Exchange Membrane Fuel Cell Stacks using Electrochemical Impedance Spectroscopy. *J. Power Sources* **2014**, *256*, 250−257.

(4) Bose, S.; Kuila, T.; Nguyen, T. X. H.; Kim, N. H.; Lau, K.-t.; Lee, J. H. Polymer Membranes for High Temperature Proton Exchange Membrane Fuel Cell: Recent Advances and Challenges. *Prog. Polym. Sci.* **2011**, *36*, 813−843.

(5) Park, J.; Wang, L.; Advani, S. G.; Prasad, A. K. Mechanical Stability of H3PO4-Doped PBI/Hydrophilic-Pretreated PTFE Membranes for High Temperature PEMFCs. *Electrochim. Acta* **2014**, *120*, 30−38.

(6) Araya, S. S.; Zhou, F.; Liso, V.; Sahlin, S. L.; Vang, J. R.; Thomas, S.; Gao, X.; Jeppesen, C.; Kær, S. K. A Comprehensive Review of PBI-Based High Temperature PEM Fuel Cells. *Int. J. Hydrogen Energy* **2016**, *41*, 21310−21344.

(7) Atanasov, V.; Gudat, D.; Ruffmann, B.; Kerres, J. Highly Phosphonated Polypentafluorostyrene: Characterization and Blends with Polybenzimidazole. *Eur. Polym. J.* **2013**, *49*, 3977−3985.
(8) Li, Q.; He, R.; Jensen, J. O.; Bjerrum, N. J. PBI-Based Polymer Membranes for High Temperature Fuel Cells- Preparation, Characterization and Fuel Cell Demonstration. *Fuel Cells* **2004**, *4*, 147−159.
(9) Quartarone, E.; Angioni, S.; Mustarelli, P. Polymer and Composite Membranes for Proton-Conducting, High-Temperature Fuel Cells: A Critical Review. *Materials* **2017**, *10*, 687.
(10) Aili, D.; Cleemann, L. N.; Li, Q.; Jensen, J. O.; Christensen, E.; Bjerrum, N. J. Thermal Curing of PBI Membranes for High Temperature PEM Fuel Cells. *J. Mater. Chem.* **2012**, *22*, 5444.
(11) Kerres, J.; Atanasov, V. Cross-linked PBI-Based High-Temperature Membranes: Stability, Conductivity and Fuel Cell Performance. *Int. J. Hydrogen Energy* **2015**, *40*, 14723−14735.
(12) Li, Q.; Pan, C.; Jensen, J. O.; Noyé, P.; Bjerrum, N. J. Cross-Linked Polybenzimidazole Membranes for Fuel Cells. *Chem. Mater.* **2007**, *19*, 350−352.
(13) Zeis, R. Materials and Characterization Techniques for High-Temperature Polymer Electrolyte Membrane Fuel Cells. *Beilstein J. Nanotechnol.* **2015**, *6*, 68−83.
(14) Henkensmeier, D.; Aili, D. Techniques for PBI Membrane Characterization. In *High Temperature Polymer Electrolyte Membrane Fuel Cells*; Li, Q., Aili, D., Hjuler, H. A., Jensen, J. O., Eds.; Springer International Publishing, 2016.
(15) Hu, M.; Li, T.; Neelakandan, S.; Wang, L.; Chen, Y. Cross-Linked Polybenzimidazoles Containing Hyperbranched Cross-Linkers and Quaternary Ammoniums as High-Temperature Proton Exchange Membranes: Enhanced Stability and Conductivity. *J. Membr. Sci.* **2020**, *593*, 117435.
(16) Luo, H.; Pu, H.; Chang, Z.; Wan, D.; Pan, H. Crosslinked polybenzimidazole via a Diels-Alder reaction for proton conducting membranes. *J. Mater. Chem.* **2012**, *22*, 20696.
(17) Liu, F.; Wang, S.; Chen, H.; Li, J.; Tian, X.; Wang, X.; Mao, T.; Xu, J.; Wang, Z. Cross-Linkable Polymeric Ionic Liquid Improve Phosphoric Acid Retention and Long-Term Conductivity Stability in Polybenzimidazole Based PEMs. *ACS Sustainable Chem. Eng.* **2018**, *6*, 16352−16362.
(18) Hao, J.; Jiang, Y.; Gao, X.; Lu, W.; Xiao, Y.; Shao, Z.; Yi, B. Functionalization of Polybenzimidazole-Crosslinked Poly(vinylbenzyl chloride) with Two Cyclic Quaternary Ammonium Cations for Anion Exchange Membranes. *J. Membr. Sci.* **2018**, *548*, 1−10.
(19) Özdemir, Y.; Özkan, N.; Devrim, Y. Fabrication and Characterization of Cross-linked Polybenzimidazole Based Membranes for High Temperature PEM Fuel Cells. *Electrochim. Acta* **2017**, *245*, 1−13.
(20) Tian, X.; Wang, S.; Li, J.; Liu, F.; Wang, X.; Chen, H.; Wang, D.; Ni, H.; Wang, Z. Benzimidazole Grafted Polybenzimidazole Cross-Linked Membranes with Excellent PA Stability for High-Temperature Proton Exchange Membrane Applications. *Appl. Surf. Sci.* **2019**, *465*, 332−339.
(21) Kerres, J. Applications of Acid-Base Blend Concepts to Intermediate Temperature Membranes. In *High Temperature Polymer Electrolyte Membrane Fuel Cells*; Li, Q., Aili, D., Hjuler, H. A., Jensen, J. O., Eds.; Springer International Publishing, 2016, pp 59−89. DOI: 10.1007/978-3-319-17082-4_4.
(22) Aili, D.; Li, Q.; Christensen, E.; Jensen, J. O.; Bjerrum, N. J. Crosslinking of Polybenzimidazole Membranes by Divinylsulfone Post-Treatment for High-Temperature Proton Exchange Membrane Fuel Cell Applications. *Polym. Int.* **2011**, *60*, 1201−1207.
(23) Wang, S.; Zhang, G.; Han, M.; Li, H.; Zhang, Y.; Ni, J.; Ma, W.; Li, M.; Wang, J.; Liu, Z.; Zhang, L.; Na, H. Novel Epoxy-Based Cross-Linked Polybenzimidazole for High Temperature Proton Exchange Membrane Fuel Cells. *Int. J. Hydrogen Energy* **2011**, *36*, 8412−8421.
(24) Xu, H.; Chen, K.; Guo, X.; Fang, J.; Yin, J. Synthesis of Hyperbranched Polybenzimidazoles and their Membrane Formation. *J. Membr. Sci.* **2007**, *288*, 255−260.
(25) Noyé, P.; Li, Q.; Pan, C.; Bjerrum, N. J. Cross-Linked Polybenzimidazole Membranes for High Temperature Proton Exchange Membrane Fuel Cells with Dichloromethyl Phosphinic Acid as a Cross-Linker. *Polym. Adv. Technol.* **2008**, *19*, 1270−1275.
(26) Harilal; Nayak, R.; Ghosh, P. C.; Jana, T. Cross-Linked Polybenzimidazole Membrane for PEM Fuel Cells. *ACS Appl. Polym. Mater.* **2020**, *2*, 3161−3170.
(27) Yang, J.; Li, Q.; Cleemann, L. N.; Jensen, J. O.; Pan, C.; Bjerrum, N. J.; He, R. Crosslinked Hexafluoropropylidene Polybenzimidazole Membranes with Chloromethyl Polysulfone for Fuel Cell Applications. *Adv. Energy Mater.* **2013**, *3*, 622−630.
(28) Wang, S.; Zhao, C.; Ma, W.; Zhang, N.; Liu, Z.; Zhang, G.; Na, H. Macromolecular cross-linked polybenzimidazole based on bromomethylated poly (aryl ether ketone) with enhanced stability for high temperature fuel cell applications. *J. Power Sources* **2013**, *243*, 102−109.
(29) Yang, J.; Aili, D.; Li, Q.; Cleemann, L. N.; Jensen, J. O.; Bjerrum, N. J.; He, R. Covalently Cross-Linked Sulfone Polybenzimidazole Membranes with Poly(vinylbenzyl chloride) for Fuel Cell Applications. *ChemSusChem* **2013**, *6*, 275−282.
(30) Venugopalan, G.; Chang, K.; Nijoka, J.; Livingston, S.; Geise, G. M.; Arges, C. G. Stable and Highly Conductive Polycation-Polybenzimidazole Membrane Blends for Intermediate Temperature Polymer Electrolyte Membrane Fuel Cells. *ACS Appl. Energy Mater.* **2020**, *3*, 573−585.
(31) Ma, W.; Zhao, C.; Lin, H.; Zhang, G.; Ni, J.; Wang, J.; Wang, S.; Na, H. High-Temperature Water-Free Proton Conducting Membranes based on Poly(arylene ether ketone) containing Pendant Quaternary Ammonium Groups with Enhanced Proton Transport. *J. Power Sources* **2011**, *196*, 9331−9338.
(32) Cho, H.; Hur, E.; Henkensmeier, D.; Jeong, G.; Cho, E.; Kim, H. J.; Jang, J. H.; Lee, K. Y.; Hjuler, H. A.; Li, Q.; Jensen, J. O.; Cleemann, L. N. Meta-PBI/Methylated PBI-OO Blend Membranes for Acid Doped HT PEMFC. *Eur. Polym. J.* **2014**, *58*, 135−143.
(33) Lee, K.-S.; Spendelow, J. S.; Choe, Y.-K.; Fujimoto, C.; Kim, Y. S. An Operationally Flexible Fuel Cell Based on Quaternary Ammonium-Biphosphate Ion Pairs. *Nat. Energy* **2016**, *1*, 447.
(34) Atanasov, V.; Lee, A. S.; Park, E. J.; Maurya, S.; Baca, E. D.; Fujimoto, C.; Hibbs, M.; Matanovic, I.; Kerres, J.; Kim, Y. S. Synergistically Integrated Phosphonated Poly(pentafluorostyrene) for Fuel Cells. *Nat. Mater.* **2021**, *20*, 370−377. Published Online: Dec. 7, 2020
(35) Lu, W.; Zhang, G.; Li, J.; Hao, J.; Wei, F.; Li, W.; Zhang, J.; Shao, Z.-G.; Yi, B. Polybenzimidazole-Crosslinked Poly(vinylbenzyl chloride) with Quaternary 1,4-Diazabicyclo (2.2.2) Octane Groups as High-Performance Anion Exchange Membrane for Fuel Cells. *J. Power Sources* **2015**, *296*, 204−214.
(36) Qaisrani, N. A.; Ma, L.; Hussain, M.; Liu, J.; Li, L.; Zhou, R.; Jia, Y.; Zhang, F.; He, G. Hydrophilic Flexible Ether Containing, Cross-Linked Anion-Exchange Membrane Quaternized with DABCO. *ACS Appl. Mater. Interfaces* **2020**, *12*, 3510−3521. Published Online: Jan. 10, 2020
(37) Park, J.-H.; Park, J.-S. KOH-Doped Porous Polybenzimidazole Membranes for Solid Alkaline Fuel Cells. *Energies* **2020**, *13*, 525.
(38) Li, Q.; He, R.; Berg, R. W.; Hjuler, H. A.; Bjerrum, N. J. Water Uptake and Acid Doping of Polybenzimidazoles as Electrolyte Membranes for Fuel Cells. *Solid State Ionics* **2004**, *168*, 177−185.
(39) Arslan, F.; Böhm, T.; Kerres, J.; Thiele, S. Spatially and Temporally Resolved Monitoring of Doping Polybenzimidazole Membranes with Phosphoric Acid. *J. Membr. Sci.* **2021**, *625*, 119145.
(40) Cho, H.; Krieg, H.; Kerres, J. Performances of Anion-Exchange Blend Membranes on Vanadium Redox Flow Batteries. *Membranes* **2019**, *9*, 31.
(41) Pan, C.; Li, Q.; Jensen, J. O.; He, R.; Cleemann, L. N.; Nilsson, M. S.; Bjerrum, N. J.; Zeng, Q. Preparation and Operation of Gas Diffusion Electrodes for High-Temperature Proton Exchange Membrane Fuel Cells. *J. Power Sources* **2007**, *172*, 278−286.
(42) Lobato, J.; Rodrigo, M. A.; Linares, J. J.; Scott, K. Effect of the Catalytic Ink Preparation Method on the Performance of High Temperature Polymer Electrolyte Membrane Fuel Cells. *J. Power Sources* **2006**, *157*, 284−292.

(43) Rau, M.; Niedergesäß, A.; Cremers, C.; Alfaro, S.; Steenberg, T.; Hjuler, H. A. Characterization of Membrane Electrode Assemblies for High-Temperature PEM Fuel Cells. *Fuel Cells* **2016**, *16*, 577−583.
(44) Cooper, K. R.; Smith, M. Electrical Test Methods for On-Line Fuel Cell Ohmic Resistance Measurement. *J. Power Sources* **2006**, *160*, 1088−1095.
(45) Kocha, S. S.; Deliang Yang, J.; Yi, J. S. Characterization of Gas Crossover and its Implications in PEM Fuel Cells. *AIChE J.* **2006**, *52*, 1916−1925.
(46) Cooper, K. R. Laboratory #4 − Fuel Crossover by Linear Sweep Voltammetry & Electrochemical Surface Area by Cyclic Voltammetry. *Fuel Cell Mag.* **2008**.
(47) *High Temperature Polymer Electrolyte Membrane Fuel Cells*; Li, Q., Aili, D., Hjuler, H. A., Jensen, J. O., Eds.; Springer International Publishing, 2016.
(48) Bandura, D. R.; Baranov, V. I.; Tanner, S. D. Detection of Ultratrace Phosphorus and Sulfur by Quadrupole ICPMS with Dynamic Reaction Cell. *Anal. Chem.* **2002**, *74*, 1497−1502.
(49) Zhang, H.; Su, S.; Chen, X.; Lin, G.; Chen, J. Performance Evaluation and Optimum Design Strategies of an Acid Water Electrolyzer System for Hydrogen Production. *Int. J. Hydrogen Energy* **2012**, *37*, 18615−18621.
(50) Lin, X.; Liang, X.; Poynton, S. D.; Varcoe, J. R.; Ong, A. L.; Ran, J.; Li, Y.; Li, Q.; Xu, T. Novel Alkaline Anion Exchange Membranes Containing Pendant Benzimidazolium Groups for Alkaline Fuel Cells. *J. Membr. Sci.* **2013**, *443*, 193−200.
(51) Hou, H.; Wang, S.; Liu, H.; Sun, L.; Jin, W.; Jing, M.; Jiang, L.; Sun, G. Synthesis and Characterization of a New Anion Exchange Membrane by a Green and Facile Route. *Int. J. Hydrogen Energy* **2011**, *36*, 11955−11960.
(52) Ogunlaja, A. S.; Hosten, E. C.; Tshentu, Z. R. The Oxidation of Dibenzothiophene using Oxidovanadium(IV)-Containing Nanofibres as Catalyst. *S. Afr. J. Chem.* **2015**, *68*, 172−180.
(53) Couture, G.; Alaaeddine, A.; Boschet, F.; Ameduri, B. Polymeric Materials as Anion-Exchange Membranes for Alkaline Fuel Cells. *Prog. Polym. Sci.* **2011**, *36*, 1521−1557.
(54) Teresa Pérez-Prior, M.; Ureña, N.; Tannenberg, M.; del Río, C.; Levenfeld, B. DABCO-Functionalized Polysulfones as Anion-Exchange Membranes for Fuel Cell Applications: Effect of Cross-linking. *J. Polym. Sci., Part B: Polym. Phys.* **2017**, *55*, 1326−1336.
(55) Yang, J. S.; Cleemann, L. N.; Steenberg, T.; Terkelsen, C.; Li, Q. F.; Jensen, J. O.; Hjuler, H. A.; Bjerrum, N. J.; He, R. H. High Molecular Weight Polybenzimidazole Membranes for High Temperature PEMFC. *Fuel Cells* **2014**, *14*, 7−15.
(56) Aili, D.; Yang, J.; Jankova, K.; Henkensmeier, D.; Li, Q. From Polybenzimidazoles to Polybenzimidazoliums and Polybenzimidazolides. *J. Mater. Chem. A* **2020**, *8*, 12854−12886.
(57) Aili, D.; Allward, T.; Alfaro, S. M.; Hartmann-Thompson, C.; Steenberg, T.; Hjuler, H. A.; Li, Q.; Jensen, J. O.; Stark, E. J. Polybenzimidazole and Sulfonated Polyhedral Oligosilsesquioxane Composite Membranes for High Temperature Polymer Electrolyte Membrane Fuel Cells. *Electrochim. Acta* **2014**, *140*, 182−190.
(58) Aili, D.; Jensen, J. O.; Li, Q. Polybenzimidazole Membranes by Post Acid Doping. In *High Temperature Polymer Electrolyte Membrane Fuel Cells*; Li, Q., Aili, D., Hjuler, H. A., Jensen, J. O., Eds.; Springer International Publishing, 2016.
(59) Li, Q. F.; Rudbeck, H. C.; Chromik, A.; Jensen, J. O.; Pan, C.; Steenberg, T.; Calverley, M.; Bjerrum, N. J.; Kerres, J. Properties, Degradation and High Temperature Fuel Cell Test of Different Types of PBI and PBI Blend Membranes. *J. Membr. Sci.* **2010**, *347*, 260−270.
(60) Kulkarni, M. P.; Thomas, O. D.; Peckham, T. J.; Holdcroft, S. High Ion Exchange Capacity, Sulfonated Polybenzimidazoles. In *Polymers for energy storage and delivery: Polyelectrolytes for batteries and fuel cells ; [Symposium on "Polymers for Energy Storage and Delivery" held in March of 2011 as part of the 241st ACS national meeting & exposition*; Page, K. A., Ed.; American Chemical Soc: Anaheim, CA, 2012; Vol. *1096*, pp 221−231. DOI: 10.1021/bk-2012-1096.ch013.ACS Symposium Series
(61) Zhang, R.; Shi, Z.; Liu, Y.; Yin, J. Synthesis and Characterization of Polybenzimidazole-Nanodiamond Hybrids via In Situ Polymerization Method. *J. Appl. Polym. Sci.* **2012**, *125*, 3191−3199.
(62) Pinar, F. J.; Rastedt, M.; Pilinski, N.; Wagner, P. Characterization of HT-PEM Membrane-Electrode-Assemblies. In *High Temperature Polymer Electrolyte Membrane Fuel Cells*; Li, Q., Aili, D., Hjuler, H. A., Jensen, J. O., Eds.; Springer International Publishing, 2016, pp 353−386. DOI: 10.1007/978-3-319-17082-4_17
(63) Galbiati, S.; Baricci, A.; Casalegno, A.; Marchesi, R. Degradation in Phosphoric Acid Doped Polymer Fuel Cells: A 6000 h Parametric Investigation. *Int. J. Hydrogen Energy* **2013**, *38*, 6469−6480.
(64) Mann, R. F.; Amphlett, J. C.; Peppley, B. A.; Thurgood, C. P. Henry's Law and the solubilities of reactant gases in the modelling of PEM fuel cells. *J. Power Sources* **2006**, *161*, 768−774.
(65) Haider, R.; Wen, Y.; Ma, Z.-F.; Wilkinson, D. P.; Zhang, L.; Yuan, X.; Song, S.; Zhang, J. High Temperature Proton Exchange Membrane Fuel Cells: Progress in Advanced Materials and Key Technologies. *Chem. Soc. Rev.* **2020**, *50*, 1138. Published Online: Nov. 27
(66) Søndergaard, T.; Cleemann, L. N.; Becker, H.; Steenberg, T.; Hjuler, H. A.; Seerup, L.; Li, Q.; Jensen, J. O. Long-Term Durability of PBI-Based HT-PEM Fuel Cells: Effect of Operating Parameters. *J. Electrochem. Soc.* **2018**, *165*, F3053−F3062.
(67) Schmidt, T. J. High-Temperature Polymer Electrolyte Fuel Cells: Durability Insights. In *Polymer Electrolyte Fuel Cell Durability*; Büchi, F. N., Inaba, M., Schmidt, T. J., Eds.; Springer: New York, 2009.
(68) Becker, H.; Reimer, U.; Aili, D.; Cleemann, L. N.; Jensen, J. O.; Lehnert, W.; Li, Q. Determination of Anion Transference Number and Phosphoric Acid Diffusion Coefficient in High Temperature Polymer Electrolyte Membranes. *J. Electrochem. Soc.* **2018**, *165*, F863−F869.
(69) Kannan, A.; Li, Q.; Cleemann, L. N.; Jensen, J. O. Acid Distribution and Durability of HT-PEM Fuel Cells with Different Electrode Supports. *Fuel Cells* **2018**, *18*, 103−112.